Neurobiology of Sleep and Circadian Rhythms 6 (2019) 24–34

Contents lists available at ScienceDirect

Neurobiology of Sleep and Circadian Rhythms

journal homepage: www.elsevier.com/locate/nbscr

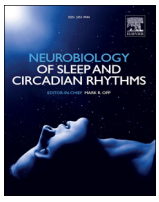

Research paper

Brain dynamics during the sleep onset transition: An EEG source localization study

Antonio Fernandez Guerrero[a,c], Peter Achermann[a,b,c,d,*]

[a] Institute of Pharmacology and Toxicology, University of Zurich, Winterthurerstrasse 190, 8057 Zurich, Switzerland
[b] The KEY Institute for Brain-Mind Research, Department of Psychiatry, Psychotherapy and Psychosomatics, University Hospital of Psychiatry, Zurich, Switzerland
[c] Neuroscience Center Zurich, University of Zurich and ETH Zurich, Zurich, Switzerland
[d] Zurich Center for Interdisciplinary Sleep Research, University of Zurich, Zurich, Switzerland

ARTICLE INFO

Keywords:
EEG sources
Transition into sleep
Homeostasis
Delta activity
Sigma activity
LORETA

ABSTRACT

EEG source localization is an essential tool to reveal the cortical sources underlying brain oscillatory activity. We applied LORETA, a technique of EEG source localization, to identify the principal brain areas involved in the process of falling asleep (sleep onset, SO). We localized the contributing brain areas of activity in the classical frequency bands and tracked their temporal evolution (in 2-min intervals from 2 min prior to SO up to 10 min after SO) during a baseline night and subsequent recovery sleep after total sleep deprivation of 40 h.

Delta activity (0.5–5 Hz) gradually increased both in baseline and recovery sleep, starting in frontal areas and finally involving the entire cortex. This increase was steeper in the recovery condition. The evolution of sigma activity (12–16 Hz) resembled an inverted U-shape in both conditions and the activity was most salient in the parietal cortex. In recovery, sigma activity reached its maximum faster than in baseline, but attained lower levels. Theta activity (5–8 Hz) increased with time in large parts of the occipital lobe (baseline and recovery) and in recovery involved additionally frontal areas. Changes in alpha activity (8–12 Hz) at sleep onset involved large areas of the cortex, whereas activity in the beta range (16–24 Hz) was restricted to small cortical areas. The dynamics in recovery could be considered as a "fast-forward version" of the one in baseline.

Our results confirm that the process of falling asleep is neither spatially nor temporally a uniform process and that different brain areas might be falling asleep at a different speed potentially reflecting use dependent aspects of sleep regulation.

1. Introduction

The process of falling asleep (sleep onset, SO) may be considered as multi-dimensional, entailing, e.g., subjective, behavioral and physiological dimensions (see Fig. 3 in Ogilvie, 2001). Frequency specific systematic EEG changes during wake-sleep transitions have been reported (Hori, 1985; Merica and Gaillard, 1992, Ogilvie, 2001). In general, a pattern of declining alpha and theta activity accompanied by increased delta activity has been observed. Not all brain areas exhibit the same frequency-specific EEG changes and not all regions change simultaneously during the wake-sleep transition (Hori, 1985; Wright et al., 1995; Berry, 1996, Ogilvie, 2001; Ferrara and De Gennaro, 2011). While occipital alpha activity is predominant in waking, the transition to sleep is accompanied first by a posterior reduction of alpha activity and second followed after SO by a spreading towards anterior areas (De Gennaro et al., 2004). Overall, the progressive temporal and spatial correlations of the EEG during the SO transition is reflected, firstly, in a fronto-parietal prominence of low frequency activity, secondly, in a maximum of spindle activity in centro-parietal areas, and finally, in a shift of alpha activity towards more anterior regions (Ferrara and De Gennaro, 2011).

An important caveat in studying the transition to sleep from waking is the criterion or definition adopted to operationalize SO based on EEG recordings in humans. Many definitions have been proposed and applied in the sleep literature; nevertheless, no general consensus has yet been established (Wright et al., 1995; Ogilvie, 2001; De Gennaro et al., 2004; Picchioni et al., 2008; Parrino et al., 2009; Prerau et al., 2014; Siclari et al., 2014; Park et al., 2015; Speth and Speth, 2016; Spiess et al., 2018). The American Academy of Sleep Medicine (AASM) defines the moment of SO as the first appearance of any 30-s epoch containing at least 15 s of any stage of sleep (Iber et al., 2007). On the other hand, the Rechtschaffen and Kales manual defined sleep onset by the first

* Corresponding author at: Institute of Pharmacology and Toxicology, University of Zurich, Winterthurerstrasse 190, 8057 Zurich, Switzerland.
E-mail address: acherman@pharma.uzh.ch (P. Achermann).

https://doi.org/10.1016/j.nbscr.2018.11.001
Received 18 July 2018; Received in revised form 25 October 2018; Accepted 26 November 2018
Available online 28 November 2018

three consecutive epochs of stage 1 (or any other stage of sleep) (Rechtschaffen and Kales, 1968).

Prerau et al. (2014) considered SO to be a continuous dynamic physiological process. They proposed a series of biological markers that can be mathematically modeled to track the SO process. These markers were the reduction of alpha power, the increase of theta and delta power and the reduction of muscle activity in a behavioral task (sustained breathing paradigm) while subjects were falling asleep. Combining these measures revealed that SO is gradual process reflecting decreasing levels of vigilance. Siclari et al. (2014) defined a time window for the SO process characterized by two different events delineating the beginning and end of the window. The beginning was associated with the disappearance of alpha activity, replaced by high frequency, low voltage activity typical of stage 1 of non-rapid eye movement (non-REM) sleep. The end of the SO window was defined by the first slow-wave sequence (FSS, generally appearing at the transition between stage 2 and stage 3 of non-REM sleep). The first slow-wave burst in the falling asleep period had to consist of more than two successive slow waves (half-wave duration > 0.5 s and > 75 μV peak-to-peak amplitude) not followed by an arousal. They investigated SO through multiple awakenings across the night and the average length of a SO window defined in this way was 9.3 ± 2.1 (SD) min.

The two studies mentioned above considered SO as a gradual process that unfolds continuously as a function of time. However, for statistical analyses of the temporal evolution in a population, data have to be aligned. Siclari et al. (2014) basically aligned the interval between the first occurrence of stage 1 and stage 3, and Prerau et al. (2014) the interval between lights out and 10 min after the last correct response in the behavioral task. However, there is no "right" definition of SO. Here, we considered the first occurrence of stage 2 (first emergence of a spindle or K-complex) as SO, indicating unequivocal signs of sleep as used in many other studies (De Gennaro et al., 2005; Magosso et al., 2007; Marzano et al., 2013; Sarasso et al., 2014; Vecchio et al., 2017). We assessed what happens during the wake-sleep transition at the cortical level by EEG source localization (exact low resolution electromagnetic tomography, eLORETA, (Pascual-Marqui et al., 2002; Pascual-Marqui et al., 2011; Pascual-Marqui et al., 2014b)), i.e. we identified the brain areas involved in the process of falling asleep. Using such a technique, it is possible to reconstruct grey matter sources that generate the observed EEG activity with maximal smoothness. Furthermore, the impact of increased sleep pressure on the SO process was investigated. The data were divided into intervals of 2 min, from 2 min prior to SO up to 10 min after SO, yielding six 2-min intervals (one before SO and five after SO). We choose a 2-min interval length as this was the interval common to all participants prior to sleep onset in the recovery condition after sleep deprivation. Average LORETA images of different frequency bands were computed for these 2-min intervals to track the temporal evolution of the SO process.

2. Methods

Source localization was performed on an existing dataset of eight healthy young males (Finelli et al., 2000; Finelli et al., 2001b). The original study was designed to investigate the effects of sleep deprivation on EEG topography. Polysomnography was performed during an adaptation night, a subsequent baseline night, and a recovery night after 40 hours of sustained wakefulness. Twenty-seven scalp EEG electrodes (extended 10–20 system; (Finelli et al., 2001b; Rusterholz and Achermann, 2011)) were recorded during baseline and recovery sleep. The EEG signals were sampled at 128 Hz (band-pass filter: 0.16–30 Hz; for additional details see (Finelli et al., 2001b)). Sleep stages were visually scored for 20-s epochs according to standard criteria (Rechtschaffen and Kales, 1968). Artifacts were identified as described in (Finelli et al., 2001b). Four-second epochs containing artifacts were replaced by the preceding epoch free of artifacts, as source localization was finally performed on 12-s epochs (i.e., three consecutive 4-s epochs). Originally, EEG data were recorded against a technical reference (reference electrode placed 5% rostral to Cz). For the subsequent processing they were re-referenced to the average reference.

The strength and distribution of the intracranial sources (squared magnitude of current source density (smCSD)) of scalp electric potential differences were estimated with eLORETA (exact low resolution electromagnetic tomography, (Pascual-Marqui et al., 2011; Pascual-Marqui et al., 2014a)) (see also Supplementary methods). We applied implementation 20160611 (most updated at the time of running this analyses) of eLORETA (available as free academic software from http://uzh.ch/keyinst/loreta). The solution space was restricted to cortical grey matter, corresponding to 6239 voxels with a spatial resolution of 5 mm. In order to compute the smCSD maps, the first step consisted of calculating cross-spectral matrices from the EEG (12-s windows). Then, the pseudoinverse rendered by LORETA transforms the frequency information at the level of the scalp to the underlying currents inside the brain at each voxel. As the analysis was performed on 2-min intervals, ten 12-s maps were averaged, finally rendering the CSD maps. The following frequency bands were analyzed: delta (0.5–5 Hz), theta (5–8 Hz), alpha (8–12 Hz), sigma (12–16 Hz) and beta (16–24 Hz).

Statistical comparisons (2-min intervals, conditions) of LORETA images were based on statistical non-parametric mapping (SnPM, (Nichols and Holmes, 2002)). This approach is based on the non-parametric randomization of the maximum-statistic over all voxels, providing an estimator for the empirical probability distribution under the null hypothesis ("no difference between conditions"), which does not need to rely on the assumption of a specific or exact statistical distribution (e.g., Gaussian), and at the same time also accounting for multiple comparisons. To this aim, a total of 5000 surrogates were generated in the application of the SnPM method. Statistical regularization (variance smoothing parameter for *t*-statistic at 5%) was performed to improve the quality of the statistics. The temporal evolution of cortical sources was investigated by comparing consecutive 2-min intervals and the 2- min intervals after SO with the one prior to SO. First, on a global level we determined how many voxels have differed between 2-min intervals and between conditions. Second, smCSD maps of selected 2-min intervals were illustrated and 2-min intervals were compared to assess the temporal changes of cortical sources underlying oscillatory activity, separately for the two conditions. Differences between conditions were assessed at the global level, i.e. how many voxels have differed between the conditions and we report the 3 brain regions that showed the largest differences.

3. Results

We investigated the temporal evolution of smCSD (mean across voxels, maps) of different frequency bands (delta, theta, alpha, sigma -spindles-, and beta), i.e. the cortical sources underlying their activity, at the transition into sleep under baseline conditions and after 40 h of sustained wakefulness (recovery sleep). Two minutes prior to SO (first occurrence of stage 2) and five 2-min intervals after SO were investigated (see Methods).

In the baseline condition, participants fell asleep within 12.0 ± 1.6 min (SEM) and significantly faster within 4.0 ± 1.2 min in recovery sleep ($P < 0.01$; Wilcoxon signed-rank test).

3.1. Temporal evolution of delta activity at sleep onset

Mean delta activity averaged across the brain (all 6239 cortical grey matter voxels) gradually increased after SO in both conditions (Fig. 1, left, blue and red line), with a steeper increase in the recovery condition. Prior to SO there was no difference in activation, however, after SO the percentage of voxels differing between the two conditions steadily increased reaching 100% at 9 min (8–10 min; Fig. 1, left, green line; SnPM). The largest leap in statistical divergence between the conditions occurred at 3 min (2–4 min) after SO, with > 70% of the

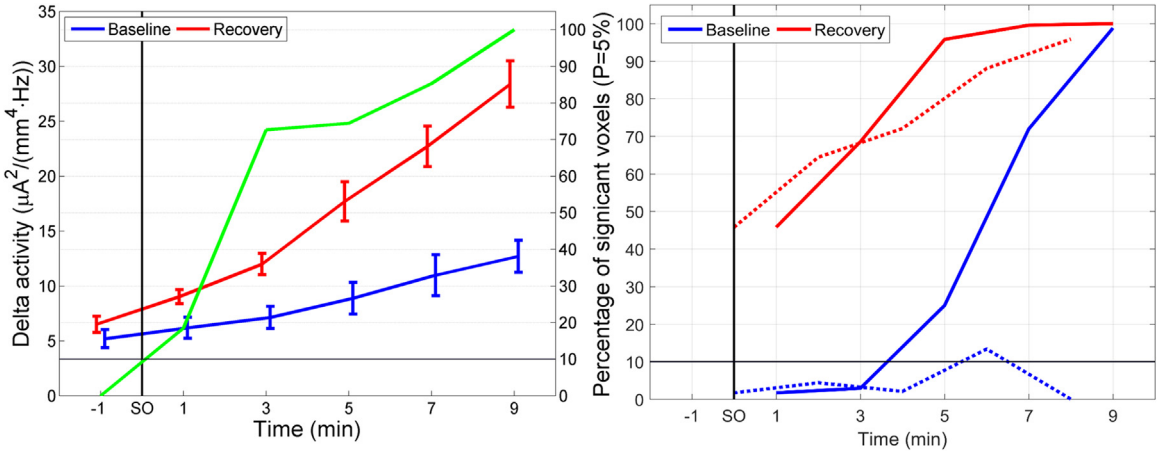

Fig. 1. Temporal evolution of delta activity. **Left panel:** Temporal evolution of delta activity (mean squared magnitude of current source density in the delta band 0.5–5 Hz; [$\mu A^2/(mm^4 Hz)$]; averaged across all voxels; left y-axis) and statistical evaluation (percentage of significantly different voxels between conditions; right y-axis) at the transition to sleep (sleep onset, SO). Blue line: mean delta activity in baseline; red line: mean delta activity in recovery; green line: percentage of voxels significantly different between recovery and baseline. **Right panel:** Percentage of voxels significantly different from the 2-min interval prior to SO (solid lines) and percentage of voxels significantly different between consecutive 2-min intervals (dashed lines). Blue lines: baseline; red lines: recovery (For interpretation of the references to color in this figure legend, the reader is referred to the web version of this article).

voxels showing higher activity in recovery sleep. Delta activity in both conditions showed a monotonic increase in the time window investigated (Fig. 1 left). Therefore, an exponential function ($\sim \exp(\alpha t)$; t, time) was fitted (Matlab function "fit" with"exp1" revealing the 95% CI). The coefficient controlling the steepness of the exponential increase was $\alpha = 0.094 \pm 0.008\ min^{-1}$ for baseline and $\alpha = 0.144 \pm 0.022\ min^{-1}$ for recovery, revealing a significant difference as the 95% CI did not overlap.

The percentage of voxels differing from the 2 min prior to SO was considerably larger in the recovery condition than in baseline. Approximately 45% of the voxels differed already in the first 2-min interval after SO (Fig. 1, right, solid lines) whereas in baseline

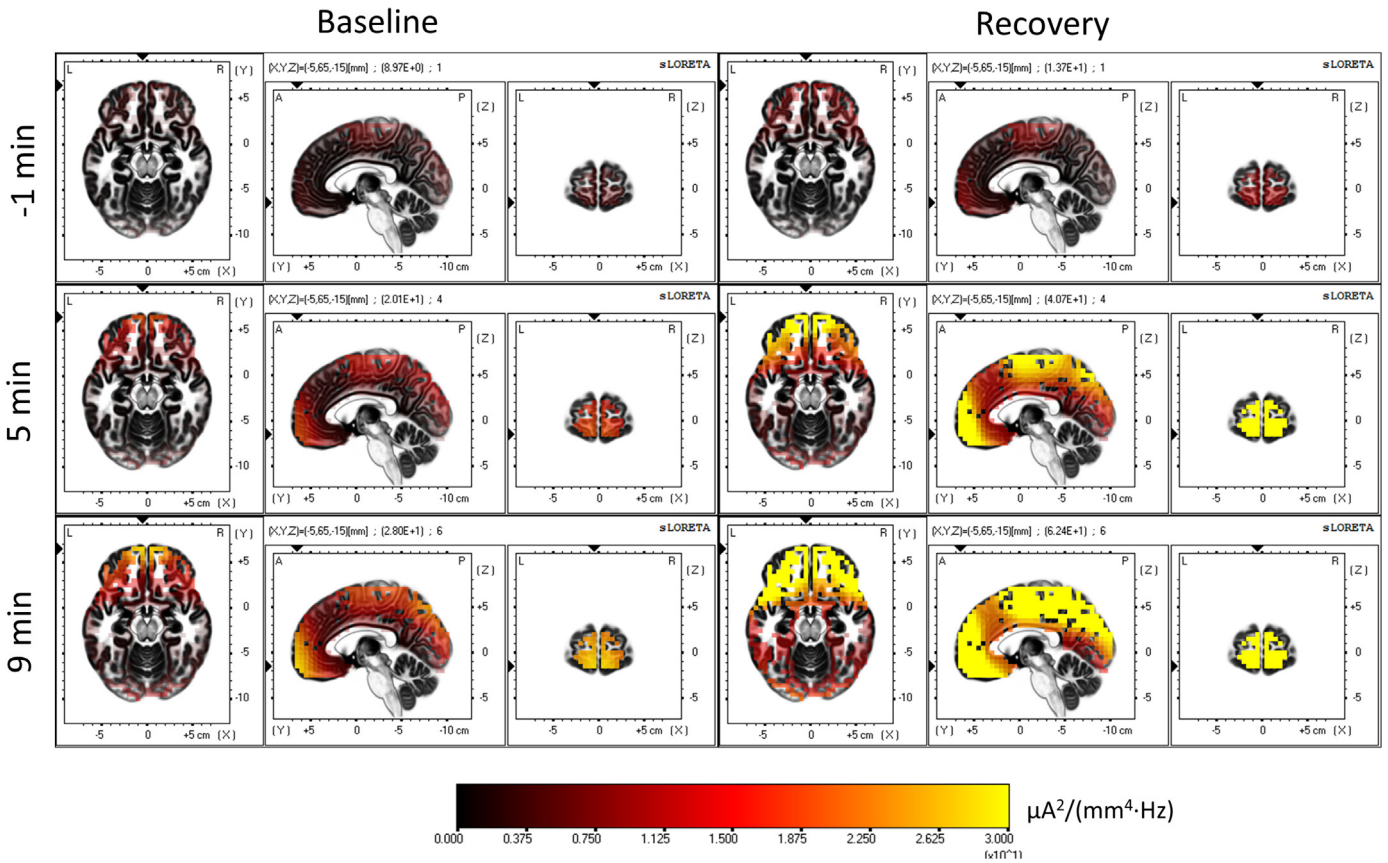

Fig. 2. Temporal evolution of the cortical sources of delta activity. LORETA source estimation of activity (squared magnitude of current source density [$\mu A^2/(mm^4$ Hz)]) in the delta band (0.5–5 Hz)). Left: baseline, right: recovery sleep. Images represent average values of the two minutes before SO (-1 min), 4–6 min (5 min) and 8–10 min (9 min) after SO. The plane coordinates were kept constant (-5, 65, -15; MNI coordinates [mm]), matching the areas showing the highest degree of delta activity during the SO transition (For interpretation of the references to color in this figure, the reader is referred to the web version of this article).

Table 1
Brodmann areas and corresponding neuroanatomical regions and lobes showing the 3 strongest activations in the delta band (0.5–5 Hz) for consecutive 2-min intervals in baseline and recovery sleep, and the strongest differences between the two conditions (sorted according to t-values).

Time interval (min)	Baseline	Recovery	Recovery minus Baseline
-2-0	BA 4 (Precentral Gyrus; Frontal Lobe) BA 3 (Postcentral Gyrus; Parietal Lobe) BA 6 (Precentral Gyrus; Frontal Lobe)	BA 11 (Medial Frontal Gyrus; Frontal Lobe) BA 11 (Superior Frontal Gyrus; Frontal Lobe) BA 6 (Superior Frontal Gyrus; Frontal Lobe)	BA 10 (Superior Frontal Gyrus; Frontal Lobe) BA 10 (Middle Frontal Gyrus; Frontal Lobe) BA 11 (Middle Frontal Gyrus; Frontal Lobe)
0–2	BA 3 (Postcentral Gyrus; Parietal Lobe) BA 4 (Precentral Gyrus; Frontal Lobe) BA 2 (Postcentral Gyrus; Parietal Lobe)	BA 11 (Medial Frontal Gyrus; Frontal Lobe) BA 11 (Superior Frontal Gyrus; Frontal Lobe) BA 3 (Postcentral Gyrus; Parietal Lobe)	BA 24* (Anterior Cingulate; Limbic Lobe) BA 32* (Anterior Cingulate; Limbic Lobe) BA 33* (Anterior Cingulate; Limbic Lobe)
2–4	BA 3 (Postcentral Gyrus; Parietal Lobe) BA 4 (Precentral Gyrus; Frontal Lobe) BA 6 (Medial Frontal Gyrus; Frontal Lobe)	BA 11 (Medial Frontal Gyrus; Frontal Lobe) BA 11 (Superior Frontal Gyrus; Frontal Lobe) BA 10 (Superior Frontal Gyrus; Frontal Lobe)	BA 6* (Middle Frontal Gyrus; Frontal Lobe) BA 32* (Cingulate Gyrus; Limbic Lobe) BA 24* (Cingulate Gyrus; Limbic Lobe)
4–6	BA 11 (Medial Frontal Gyrus; Frontal Lobe) BA 11 (Superior Frontal Gyrus; Frontal Lobe) BA 10 (Superior Frontal Gyrus; Frontal Lobe)	BA 11 (Medial Frontal Gyrus; Frontal Lobe) BA 11 (Superior Frontal Gyrus; Frontal Lobe) BA 10 (Superior Frontal Gyrus; Frontal Lobe)	BA 6* (Superior Frontal Gyrus; Frontal Lobe) BA 6* (Middle Frontal Gyrus; Frontal Lobe) BA 32* (Medial Frontal Gyrus; Frontal Lobe)
6–8	BA 7 (Precuneus; Parietal Lobe) BA 3 (Postcentral Gyrus; Parietal Lobe) BA 5 (Postcentral Gyrus; Parietal Lobe)	BA 11 (Medial Frontal Gyrus; Frontal Lobe) BA 11 (Superior Frontal Gyrus; Frontal Lobe) BA 10 (Superior Frontal Gyrus; Frontal Lobe)	BA 32* (Cingulate Gyrus; Limbic Lobe) BA 24* (Cingulate Gyrus; Limbic Lobe) BA 9* (Inferior Frontal Gyrus; Frontal Lobe)
8–10	BA 11 (Medial Frontal Gyrus; Frontal Lobe) BA 11 (Superior Frontal Gyrus; Frontal Lobe) BA 10 (Superior Frontal Gyrus; Frontal Lobe)	BA 11 (Medial Frontal Gyrus; Frontal Lobe) BA 11 (Superior Frontal Gyrus; Frontal Lobe) BA 10 (Superior Frontal Gyrus; Frontal Lobe)	BA 32* (Cingulate Gyrus; Limbic Lobe) BA 6* (Medial Frontal Gyrus; Frontal Lobe) BA 8* (Medial Frontal Gyrus; Frontal Lobe)

* $P < 0.05$, areas that were stronger activated after sleep deprivation than during baseline.

differences started to emerge 5 min after SO (4–6 min), indicating that delta activity increased faster in recovery than baseline. In the last 2-min interval, in both conditions, activity in all voxels was larger than before SO. Comparing consecutive 2-min intervals, there was basically no difference in baseline, however, during recovery large differences started to emerge immediately after SO (Fig. 1, right, dashed lines) again, indicative of a faster increase.

Fig. 2 illustrates the gradual spatial buildup of the cortical sources of delta activity (two minutes before the transition (-1 min), 4–6 (5 min) and 8–10 min (9 min) after SO), both, in baseline (left) and recovery sleep (right). To facilitate the visual temporal tracking, the plane coordinates at the different time points were kept constant matching the areas showing the highest degree of delta activity during the SO transition. Areas with highest delta activity were located in the frontal and the parietal lobe, specifically, in BA 11 (most of the prefrontal cortex; Table 1) and BA 3 (the postcentral gyrus). Delta activity in recovery sleep rose faster, including the parietal cortex, but the highest activity was still located in the frontal lobe, where the effects of sleep

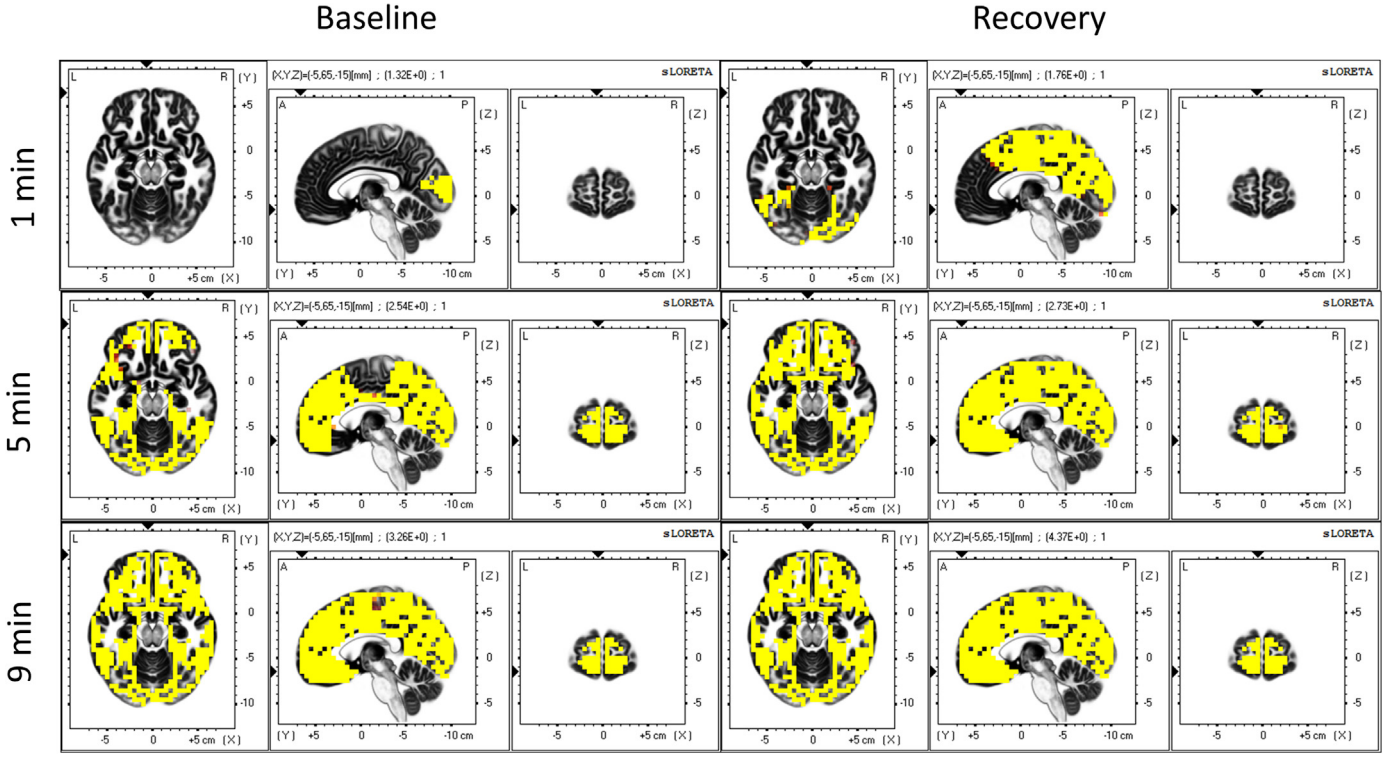

Fig. 3. Statistical assessment of the temporal evolution of the cortical sources of delta activity (0.5–5 Hz). Left: baseline, right: recovery sleep. Yellow areas represent voxels that showed higher delta activity after SO (*t*-values at $P < 0.05$). Minutes 0–2 (1 min), 4–6 (5 min) and 8–10 (9 min) were compared to the two min prior to SO (-2 to 0 min). Coordinates of the planes are as in Fig. 2 (For interpretation of the references to color in this figure legend, the reader is referred to the web version of this article).

deprivation were most noticeable.

Fig. 3 reveals the spatial statistical evaluation of the time course of delta activity. Intervals 0–2 (1 min), 4–6 (5 min), and 8–10 min (9 min) were compared to the two min prior to SO (-1 min; $P < 0.05$, yellow). Recovery exhibited a faster rate of increase with almost 100% of the voxels being different than the 2 minutes before SO already 4–6 min after the transition (Fig. 1, right, solid red line), whereas baseline was delayed and converged to the same level as recovery around 8–10 min after SO. The most salient region in both conditions is BA 11 in the frontal lobe (Table 1), but the changes finally extend to the entire cortex.

Table 1 illustrates the three brain regions with the highest delta activity during baseline and recovery of consecutive 2-min intervals, and the brain areas with the largest statistical difference (as measured by *t*-values) between recovery and baseline (activity in recovery > baseline). For example, in the 2-min interval prior to SO of baseline, Brodmann area 4 showed the highest delta activity, Brodmann area 3 the second highest and Brodmann area 6 the third highest level. The corresponding neuroanatomical regions and lobes are also indicated. It is worthy to note that particular Brodmann areas may extend spatially encompassing various neuroanatomical locations, not only a single one. This explains the repetitions occurring in Table 1, e.g., BA 11, an important area involved in decision making, planning and reasoning (Rogers et al., 1999), including part of the medial frontal gyrus as well as parts of the superior frontal gyrus in the frontal lobe. Overall, Table 1 supports the notion that a major effect of sleep deprivation was a speeding up of the temporal dynamics of delta activity compared to baseline sleep. We observed that recovery sleep resulted in a temporally accelerated activation of brain areas compared to baseline, showing its highest delta activity in BA 11 and BA 10 (i.e., areas of the prefrontal cortex), stabilizing around 2–4 min after SO. In contrast, baseline dynamics are delayed relative to recovery sleep, as activations in BA 11 and 10 appeared for the first time around 4–6 min after SO, i.e., one 2-min interval later than in recovery. Around 6–8 min after SO, activations in baseline exhibited a shift of its main activated areas to the parietal lobe, but finally returned back to the frontal lobe 8–10 min after SO. Furthermore, BA 11 in recovery even appears activated before SO, although with different regions for second and third Brodmann areas of highest activity, hence highlighting the role of this prefrontal area in generating delta activity.

3.2. Temporal evolution of sigma (spindle) activity at sleep onset

Next, we investigated the temporal evolution of the cortical sources underlying spindle (sigma) activity (12–16 Hz) at the transition into sleep. Highest mean smCSD values in the sigma band did not exceed 0.35 $\mu A^2/(mm^4$ Hz), i.e., were typically two orders of magnitude lower than for delta activity (approximately 30 $\mu A^2/(mm^4$ Hz); Figs. 1 and 4, left panels, blue and red lines).

Mean sigma activity gradually increased after SO in both conditions (Fig. 4, left, blue and red line) and peaked around 7 min after SO in baseline and at 3 min in recovery. The largest increase occurred in the first 2-min interval after SO, as expected according to our definition of SO (stage 2; first occurrence of sleep spindles or a K-complex). Activations did not differ between conditions, i.e. hardly any voxels differed between the two conditions (Fig. 4, left, green line).

The percentage of voxels differing from the 2 min prior to SO peaked at 5 min in baseline and at 3 min in recovery and was substantially larger in baseline (Fig. 4, right, solid lines). In summary, in baseline sleep larger brain areas produced spindle activity and, furthermore, were able to sustain it for a longer time. Consecutive 2-min intervals only showed a difference in the percentage of voxels activated at the transition and in the last 2-min interval in both conditions (Fig. 4, right, dashed lines), corresponding to an increase in sigma activity after SO (0–2 min) and a decrease in the last 2-min interval (8–10 min).

Fig. 5 depicts the smCSD maps illustrating the underlying generators of spindle activity. They highlight particularly the parietal lobe, both in baseline and recovery, as the most prominent region in the generation of cortical spindles. However, there were some additional contributions, although more diffuse, resulting from posterior parts of the frontal lobe (such as the postcentral gyrus) and, towards the back of the brain, extending marginally into the cuneus and the lingual gyrus of the occipital cortex (Table 2).

The temporal evolution of spatial aspects of sigma activity is illustrated in Fig. 6. Minutes 0–2 (1 min), 4–6 (5 min) and 8–10 (9 min) after SO were compared to the two minutes prior to SO (-2 to 0 min). The baseline condition (Fig. 6, left) revealed in general more widespread statistical changes across the brain after SO than during recovery, i.e. covering larger areas. The capacity to generate spindles was reduced by sleep deprivation (Fig. 6, right). It is worthy to note the symmetry between the left and right hemispheres in their statistical topographical properties, as shown by the coronal plane section (right map of each row). The most consistent regions showing changes in sigma activity appeared along the parietal lobe and its cortical surroundings, with some contributions of frontal areas (Table 2).

A further aspect of the temporal evolution, comparing consecutive 2-min intervals, is depicted in Fig. 7 comparing 8–10 min after SO with the preceding 2 min. The first 2 min after SO were already illustrated in Fig. 6. These are the only two intervals showing at least 10% of all voxels changed (Fig. 4, right, dashed curves). The first 2 min after SO showed increased sigma activity (Fig. 6, top row), the last 2 min a decrease (Fig. 7). Fig. 7 is also consistent with Figs. 5 and 6, showing again that the areas playing a predominant role for the sigma activity at SO were mainly located in the parietal lobe. Table 2 lists the neuroanatomical location of the most salient regions appearing in Figs. 5–7. Both for baseline and recovery, the most relevant Brodmann areas were, rated in order of the strength of their activity levels: BA 3, 4 and 6. BA 3 and 4 are located in between the superior parietal lobe and the posterior part of the frontal lobe, near the paracentral lobe (part of BA 4) and the central sulcus; BA 6 is on the posterior edge of the frontal lobe. Table 2 also reveals that for the second 2-min interval after SO (2–4 min after SO) and fourth interval (6–8 min after SO), there was an exact match of the three most activated Brodmann areas in baseline and recovery. Additionally, by counting the lobes appearing in each column, the table suggests that, although sigma activity is principally originating from centro-parietal regions, for baseline, there is a small preference towards more anterior areas (particularly to BA 6, on the edge of the frontal lobe), whereas for recovery, the preference goes more towards posterior areas (particularly to BA 4, encompassing the central sulcus).

3.3. Temporal evolution of alpha activity at sleep onset

Alpha activity (8–12 Hz) exhibited a progressive increase with time reaching a plateau during the last five minutes (Fig. S1, blue and red lines). This time course was observed in both conditions (particularly in parieto-occipital areas), but in recovery the increase was faster and a higher asymptotic value than in baseline was reached. Supplementary Fig. S2 indicates that strongest alpha activity was observed in BA 7, the precuneus (on the edge between the superior parietal and occipital lobes). The prominent role of the precuneus in the alpha band is consistent with the sleep onset process, since it is an area previously linked to visual imagery (i.e., it might be related to hypnagogic hallucinations) and critical for conscious information processing (Vogt and Laureys, 2005). More detailed information and descriptions can be found in Supplementary material.

3.4. Temporal evolution of beta activity at sleep onset

Beta activity (16–24 Hz) showed a decrease with time in both conditions, but with a faster decline in recovery (Fig. S4, blue and red line). However, less than 10% of the voxels differed between the conditions

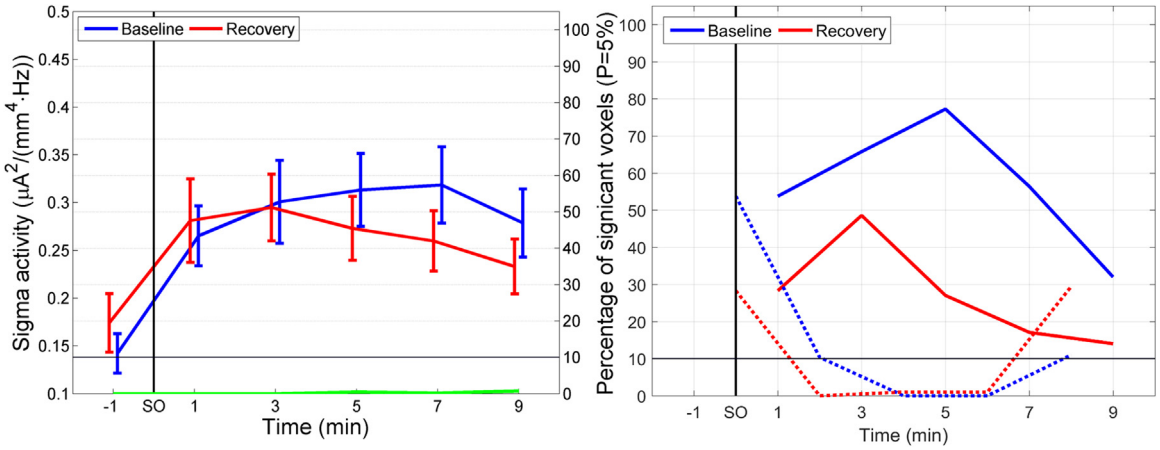

Fig. 4. Temporal evolution of sigma activity. **Left panel:** Temporal evolution of sigma activity (mean squared magnitude of current source density in the sigma band (12–16 Hz) [$\mu A^2/(mm^4 \cdot Hz)$]; averaged across all voxels; left y-axis) and statistical evaluation (percentage of significantly different voxels between conditions; right y-axis) at the transition to sleep (sleep onset, SO). Blue line: mean sigma activity in baseline; red line: mean sigma activity in recovery; green line: percentage of voxels significantly different between recovery and baseline. **Right panel:** Percentage of voxels significantly different from the 2-min interval prior to SO (solid lines) and percentage of voxels significantly different between consecutive 2-min intervals (dashed lines) (For interpretation of the references to color in this figure legend, the reader is referred to the web version of this article).

(Fig. S4, green line). The most salient regions (based on maximum smCSD values) were in the occipital and parietal lobes. Supplementary Figs. S5 and S6 reveal topographically the decrease of beta activity in grey matter voxels and indicate that for the recovery condition beta activity dissipated quicker. As for alpha activity, BA 7 (the precuneus) was also involved in the generation of beta activity. In contrast, beta activity was decreasing while alpha activity was increasing. Other major areas involved in the generation of beta activity were BA 6 and 4. More detailed information is provided in Supplementary material.

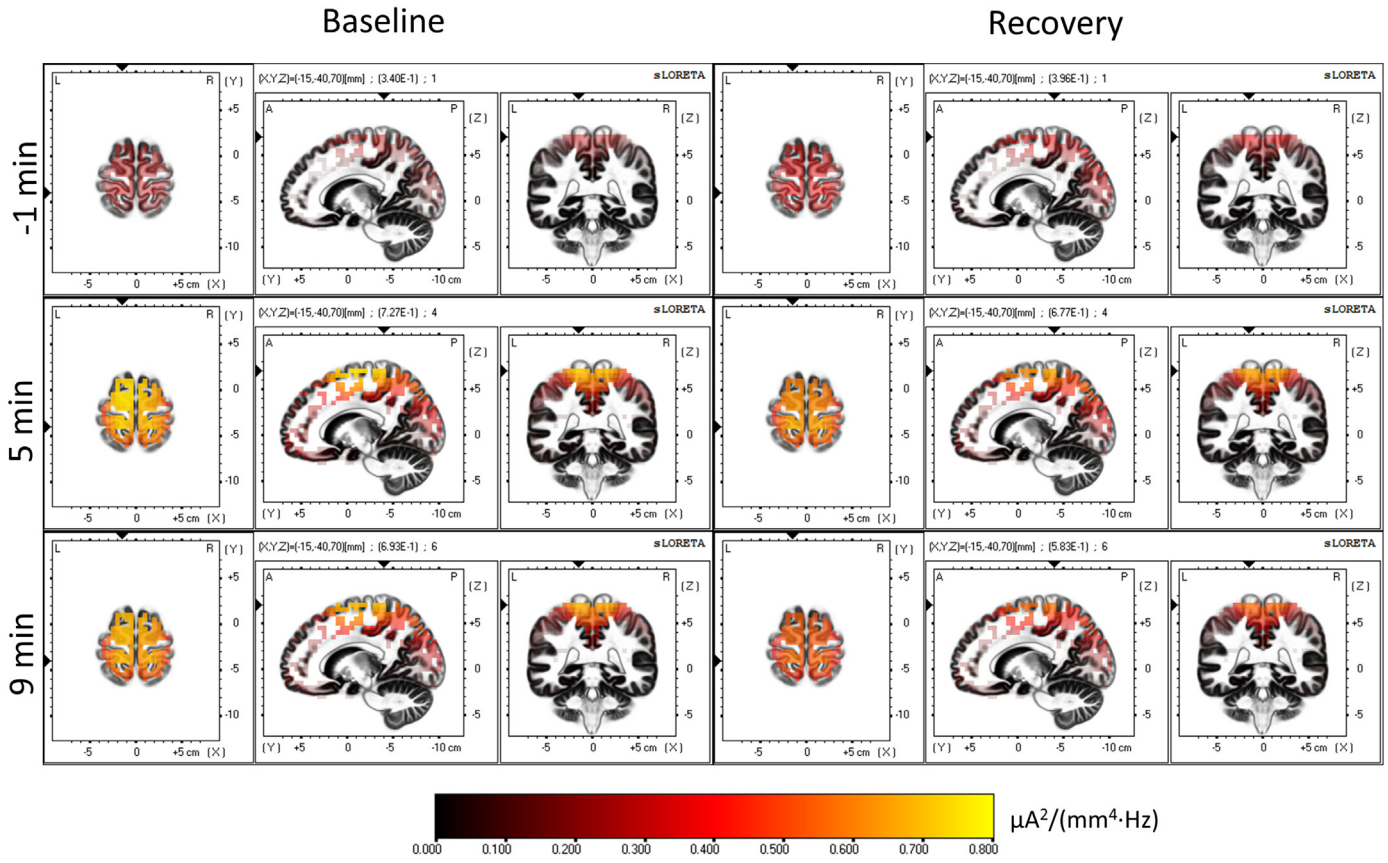

Fig. 5. Temporal evolution of the cortical sources of sigma activity. LORETA source estimation (squared magnitude of current source density [$\mu A^2/(mm^4\ Hz)$] in the sigma band (12–16 Hz). Left: baseline, right: recovery sleep. Images represent average values of the two minutes before SO (-1 min), 4–6 min (5 min) and 8–10 min (9 min) after SO. The plane coordinates were chosen to best match the most active brain regions (-15, -40, 70 in MNI coordinates [mm]) (For interpretation of the references to color in this figure, the reader is referred to the web version of this article).

Table 2
Brodmann areas and corresponding neuroanatomical regions and lobes showing the 3 strongest activations in the sigma band (12–16 Hz) for consecutive 2-min intervals in baseline and recovery sleep, and the strongest differences between the two conditions (sorted according to t-values).

Time interval (min)	Baseline	Recovery	Recovery minus Baseline
-2–0	BA 4 (Precentral Gyrus; Frontal Lobe) BA 3 (Postcentral Gyrus; Parietal Lobe) BA 4 (Postcentral Gyrus; Frontal Lobe)	BA 7 (Precuneus; Parietal Lobe) BA 19 (Cuneus; Occipital Lobe) BA 19 (Precuneus; Parietal Lobe)	BA 19 (Fusiform Gyrus; Occipital Lobe) BA 18 (Lingual Gyrus; Occipital Lobe) BA 19 (Lingual Gyrus; Occipital Lobe)
0–2	BA 3 (Postcentral Gyrus; Parietal Lobe) BA 4 (Precentral Gyrus; Frontal Lobe) BA 6 (Precentral Gyrus; Frontal Lobe)	BA 4 (Precentral Gyrus; Frontal Lobe) BA 6 (Superior Frontal Gyrus; Frontal Lobe) BA 6 (Medial Frontal Gyrus; Frontal Lobe)	BA 9 (Middle Frontal Gyrus; Frontal Lobe) BA 9 (Superior Frontal Gyrus; Frontal Lobe) BA 10 (Middle Frontal Gyrus; Frontal Lobe)
2–4	BA 4 (Precentral Gyrus; Frontal Lobe) BA 3 (Postcentral Gyrus; Parietal Lobe) BA 6 (Superior Frontal Gyrus; Frontal Lobe)	BA 4 (Precentral Gyrus; Frontal Lobe) BA 3 (Postcentral Gyrus; Parietal Lobe) BA 6 (Superior Frontal Gyrus; Frontal Lobe)	BA 18 (Middle Occipital Gyrus; Occipital Lobe) BA 17 (Cuneus; Occipital Lobe) BA 19 (Middle Occipital Gyrus; Occipital Lobe)
4–6	BA 6 (Superior Frontal Gyrus; Frontal Lobe) BA 6 (Medial Frontal Gyrus; Frontal Lobe) BA 6 (Precentral Gyrus; Frontal Lobe)	BA 3 (Postcentral Gyrus; Parietal Lobe) BA 4 (Precentral Gyrus; Frontal Lobe) BA 4 (Paracentral Lobe; Parietal Lobe)	BA 47* (Inferior Frontal Gyrus; Frontal Lobe) BA 11* (Inferior Frontal Gyrus; Frontal Lobe) BA 11* (Middle Frontal Gyrus; Frontal Lobe)
6–8	BA 3 (Postcentral Gyrus; Parietal Lobe) BA 4 (Precentral Gyrus; Frontal Lobe) BA 4 (Paracentral Lobe; Parietal Lobe)	BA 3 (Postcentral Gyrus; Parietal Lobe) BA 4 (Precentral Gyrus; Frontal Lobe) BA 4 (Paracentral Lobe; Parietal Lobe)	BA 31* (Cingulate Gyrus; Limbic Lobe) BA 23* (Posterior Cingulate; Limbic Lobe) BA 30* (Posterior Cingulate; Limbic Lobe)
8–10	BA 6 (Superior Frontal Gyrus; Frontal Lobe) BA 6 (Medial Frontal Gyrus; Frontal Lobe) BA 3 (Postcentral Gyrus; Parietal Lobe)	BA 3 (Postcentral Gyrus; Parietal Lobe) BA 4 (Precentral Gyrus; Frontal Lobe) BA 4 (Postcentral Gyrus; Frontal Lobe)	BA 6* (Precentral Gyrus; Frontal Lobe) BA 4* (Precentral Gyrus; Frontal Lobe) BA 18* (Cuneus; Occipital Lobe)

* $P < 0.05$, areas that were less activated after sleep deprivation than during baseline. Significant differences appeared only in the last two 2-min intervals.

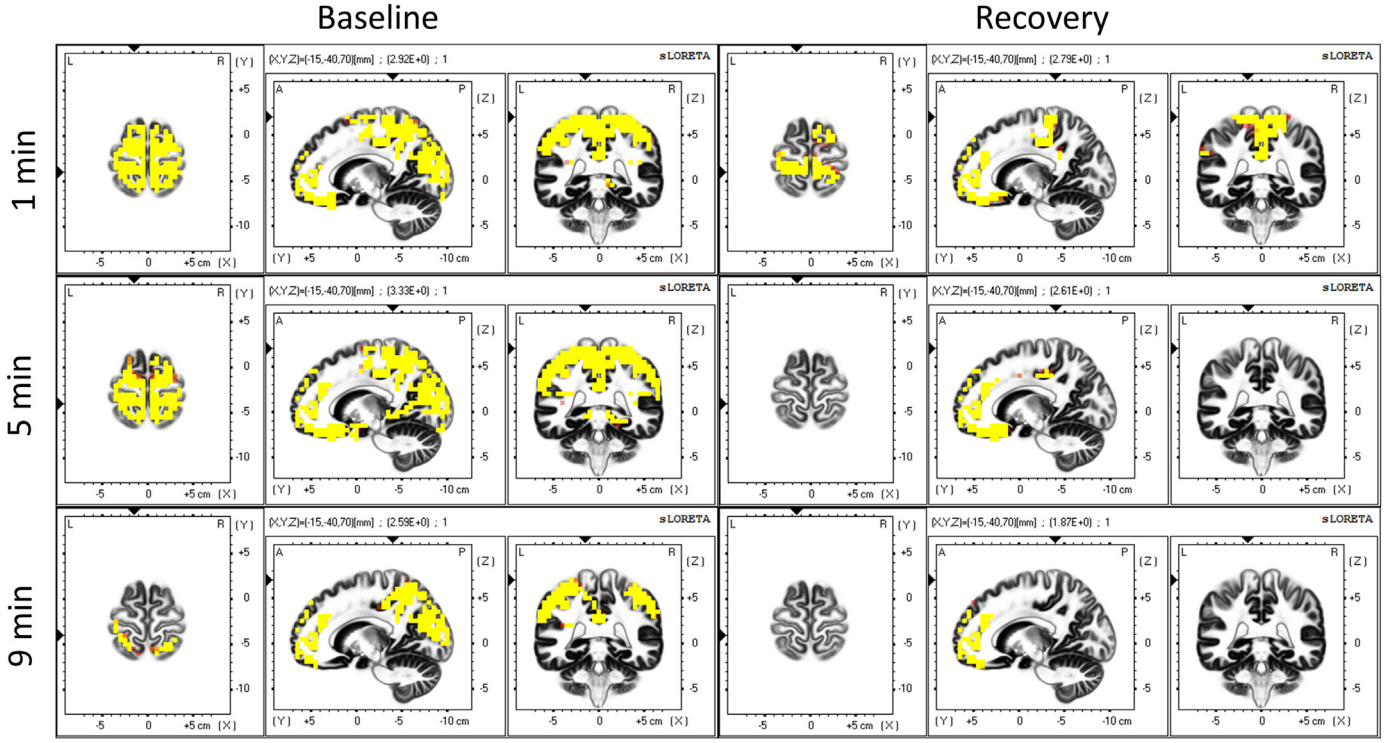

Fig. 6. Statistical assessment of the temporal evolution of the cortical sources of sigma activity (12–16 Hz). Left: baseline, right: recovery sleep. Yellow areas represent voxels that showed higher sigma activity after SO (*t*-values at $P < 0.05$). Minutes 0–2 (1 min), 4–6 (5 min) and 8–10 (9 min) were compared to the two minutes prior to SO (-2 to 0 min). Coordinates of the planes are as in Fig. 5 (For interpretation of the references to color in this figure legend, the reader is referred to the web version of this article).

3.5. Temporal evolution of theta activity at sleep onset

Similar to alpha activity, theta activity (5–8 Hz) increased in both conditions until a plateau was reached (Fig. S7, blue and red line). The plateau levels were higher in recovery than baseline. Theta activity did not differ between conditions prior to SO (Figs. S7, green line and S8, upper row), whereas there was a considerable statistical separation after SO (Figs. S7 to S9), indicating that the maximal statistical separation between conditions happened at 5 min after SO (with more than 60% of the voxels being significantly different). The most salient areas in the smCSD maps were again the precuneus (BA 7), in the superior parietal lobe, followed by the cuneus (BA 19), in the occipital lobe. For more detailed information, see Supplementary material.

4. Discussion

We investigated the strength and distribution of the intracranial sources of activity of different frequency bands at the transition into

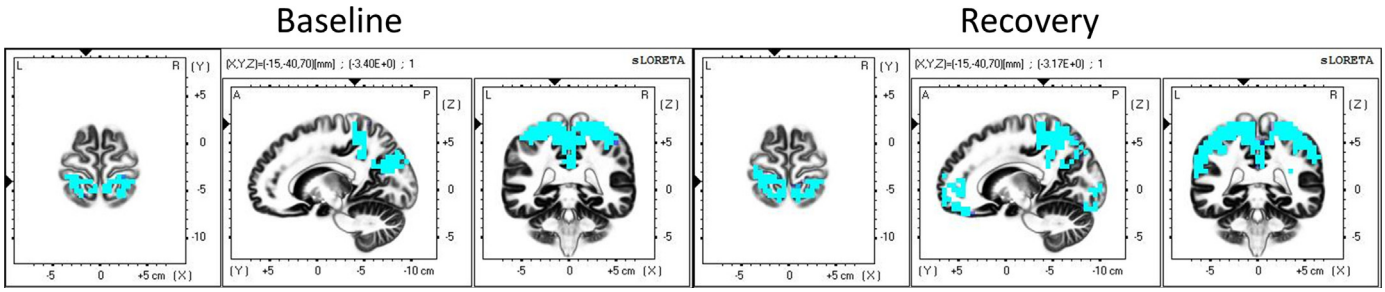

Fig. 7. Statistical assessment (contrast of the last two 2-min intervals) of cortical sources of sigma activity (12–16 Hz). Left: baseline, right: recovery sleep. Blue areas represent voxels that decreased in activity in the statistical contrast (*t*-values at $P < 0.05$). Minutes 8–10 (last interval) were compared to the previous two min, 6–8 min after SO. Coordinates of the planes are as in Fig. 5 (For interpretation of the references to color in this figure legend, the reader is referred to the web version of this article).

sleep (first ten minutes) and how they are affected by increased sleep pressure (total sleep deprivation). We applied LORETA (Pascual-Marqui et al., 2002) to estimate the underlying sources of brain electrical activity. According to our alignment of the data, we basically compared stage 1 (2 min prior to SO) with stage 2 (in baseline) and with stage 2 followed by SWS (in recovery).

Our results confirm that the process of falling asleep is neither spatially nor temporally a uniform process (Magnin et al., 2010; Prerau et al., 2014; Siclari et al., 2014). Changes in delta and alpha activity at sleep onset involved large areas of the cortex, whereas activity in the beta range was restricted to small cortical areas and sigma activity was most salient in the parietal cortex. Increased sleep pressure due to sleep deprivation altered the dynamics in recovery sleep leading to a kind of "fast-forward", i.e., an accelerated version of the baseline dynamics appearing in most frequency bands.

4.1. Delta activity

Delta activity averaged across all cortical grey matter voxels showed an exponential increase at the beginning of sleep (Fig. 1, left, blue and red lines) which was faster after sleep deprivation. This finding is in line with early studies examining the buildup of SWA of a single EEG derivation (C3A2; (Dijk et al., 1990)). Siclari et al. (2014) demonstrated a similar time course of slow wave density and hypothesized that the observed temporal evolution resulted from two distinct synchronization processes, first dominated by "Type I" slow waves (mediated by subcortical arousal promoting structures in the pons), followed by "Type II" slow waves (originating from cortico-cortical synchronization processes). Children however, did not yet show this two temporally dissociated synchronization processes (Spiess et al., 2018). With our approach we could not dissociate the two types of slow waves.

Other studies have shown that anterior areas are the first to exhibit slow waves activity, and the onset of these waves is accelerated in recovery sleep (De Gennaro et al., 2005; Ferrara and De Gennaro, 2011). Already in 1949, Brazier (Brazier, 1949) reported a shift of focus from occipital to frontal regions when transitioning from waking to sleep. Gradually more brain regions showed increased slow wave activity compared to the pre-sleep interval reaching 100% after 9 min in baseline and almost 100% at 5 min in recovery (Fig. 1), like in the study of Marzano et al. (2013) who also observed an involvement of all cortical areas up to 7 Hz based on EEG topography. After 3 min more than 70% of the voxels differed in intensity between the conditions reaching 100% in the last 2-min interval. Brain regions got gradually activated (as assessed by showing the largest smCSD values), starting with BA 3 (postcentral gyrus in the parietal lobe), followed BA 6 (premotor cortex and supplementary motor cortex in the frontal lobe) and finally BA 10 and 11 (frontopolar cortex in the frontal lobe) (Figs. 2 and 3; Table 1). Similarly, Siclari et al. (2014) reported that the brain regions predominantly involved in the rise of delta activity were located in the anterior medial prefrontal cortex, primary cortex and posteromedial parietal cortex.

Our spatial analysis revealed that the homeostatic effects were accentuated over the frontal lobe. These regions experience a higher computational load due to daily activities, such as decision making, executive functions and emotional regulation (Rogers et al., 1999; Nir et al., 2011; Ikeda et al., 2015). Power spectral density increased progressively along the 10 intervals covered (approximately 10 min), being more prominent in the frontal lobe and central areas of the parietal lobe (Siclari et al., 2014). The most frequent origins of slow waves at the beginning of SO corresponded to the primary motor and sensory cortices (extending also into dorsolateral prefrontal cortex), the inferior frontal gyrus and the posteromedial parietal cortex (posterior cingulate and precuneus). Cortical involvement maps (the amount of current produced by different cortical areas) also highlighted the major role exerted by the frontal lobe at the beginning of the SO transition. Thus, the areas reported by Siclari et al. (2014) are concordant with our findings (Figs. 2 and 3 and Table 1). Towards the second half of the time interval investigated, the origin of slow waves spread evenly throughout the cortex (Siclari et al., 2014), which is also in correspondence with the spatially homogenous spatial maps we observed in the last 2-min interval.

De Gennaro et al. (2000, 2001b) investigated the behavior of power spectral density along the SO transition. Based on the scalp EEG topography, they found that in a five min interval before SO (defined as the first appearance of a spindle or K-complex), the low frequency range (< 7 Hz) was characterized by an anterior-posterior gradient, in which central, frontal and frontopolar areas standing out the most. Parietal areas also showed more prominence than occipital areas. On the other hand, in a five min interval after SO, power was significantly larger in fronto-central scalp locations. They argued that the prevalence of EEG power in frontal and central areas indicate that these areas are the first to synchronize its oscillatory activity during the SO process, as also confirmed in their later study (Marzano et al., 2013). These results are consistent with what we observed through source localization. Another study by the same authors confirmed and extended the previous results (De Gennaro et al., 2001a). In the low frequency range (1–6 Hz), a linear increase of log power spectral density with time was observed consistent with the exponential dynamics of delta activity we observed at the SO transition.

4.2. Sigma activity

Sigma activity (12–16 Hz) followed an inverted U-shape along the SO transition, peaking at a different time interval depending on the level of sleep pressure (quicker in recovery; Fig. 4) and showing, at the beginning of the SO transition, a concomitant rise with delta activity and an inverse relationship with delta at the end of the investigated time window. This type of behavior has been previously observed in single channel EEG studies (Aeschbach and Borbély, 1993; Aeschbach et al., 1997). Also Siclari et al. reported such a temporal evolution of

spindle density and the percentage of scalp involvement in spindle activity across channels (Siclari et al., 2014). Moreover, the different time course of slow wave and spindle density lead them to postulate three phases characterizing the SO period (Siclari et al., 2014).

During recovery, spindle activity was diminished compared to baseline in accordance with previous reports (Borbély et al., 1981; De Gennaro et al., 2001a).

De Gennaro and Ferrara (2003) investigated the effect of two nights of selective slow wave deprivation on spindle density (12–15 Hz) at SO. An inverse relationship between delta and sigma activity, such that an enhancement of delta activity accompanied by a decrease of sigma activity was observed. A simple topographical analysis of sleep spindle density of the channels studied revealed spatial heterogeneity of spindle occurrence, where centro-parietal areas revealed stronger spindle activity, followed by the frontal lobe, and lastly the occipital cortex. These results were corroborated by our own analyses (Fig. 4, evolution of mean spindle activity; Figs. 5 and 6 as well as Table 2 for spatial aspects).

Also the results of spindle activity in the study performed by Siclari et al. (2014) were largely congruent with our own findings. The spindle density (number of spindles per minute) underwent an initial increase until reaching a maximum (appearing earlier and more pronounced on anterior and central regions), which then experienced a moderate decrease during the last minutes of the nearly 10-min window investigated. Furthermore, the authors distinguished between slow frontal and fast centro-parietal spindles, the latter corresponding to our sigma activity (12–16 Hz). The most frequent origins of spindles assessed by Siclari et al. (2014) were located in the anterior cingulate cortex and the dorsolateral and medial prefrontal cortex for frontal (slow) spindles, whereas they were located in the precuneus and posterior cingulate cortex for centro-parietal (fast) spindles (all these areas also appeared to be involved in our study; Figs. 5 and 6, Table 2, particularly in the baseline condition).

Commonly, fast and slow spindles are dissociated (De Gennaro and Ferrara, 2003). We focused on fast spindle activity (12–16 Hz). It is, however, difficult to distinguish slow spindles from alpha activity, in particular alpha activity occurring in NREM sleep (Scheuler et al., 1988, 1993; Olbrich and Achermann, 2005). Additionally, we investigated the changes in the alpha band (8–12 Hz), which comprises both NREM alpha and slow spindle activity (see below).

Anderer et al. and Del Felice et al. investigated the cortical sources of sleep spindles using LORETA (Anderer et al., 2001; Del Felice et al., 2014). They localized slow (10–12 Hz) and fast (12–14 Hz) spindles. Fast spindles appeared more scattered throughout the brain, including the medial and inferior frontal gyrus, inferior parietal lobule, middle temporal gyrus and lingual gyrus in the occipital cortex. The reported brain areas are comparable with our own results. Slow spindles were mostly localized along the frontal lobe (in particular, medial and inferior frontal gyri). With increasing time into sleep, alpha activity (including slow spindles) revealed also the recruitment of the frontal lobe in our study.

4.3. Other frequency bands

In the alpha band (8–12 Hz), activity gradually increased along the SO transition until reaching a steady state involving 50% to 80% of the cortex. We did not see an initial drop of alpha activity as our 2-min interval before SO was basically composed of stage 1 sleep. The observed rise was initially pronounced in the occipital cortex and parts of the parietal lobe and with increasing time the involvement of the frontal lobe became evident like the progressive increase of alpha activity with a centro-frontal maximum observed by Marzano et al. (2013). During recovery sleep a faster increase was present and higher levels were reached. This observation is indicative that we rather captured NREM sleep alpha than slow spindles, as spindle activity is generally reduced with increased sleep pressure.

The average temporal behavior of the theta band (4–8 Hz) was similar to the one of the alpha band. Theta activity increased with time in large parts of the occipital lobe (baseline and recovery). Also other groups reported an occipital or posterior prevalence of theta activity (Wright et al., 1995; Marzano et al., 2013; Park et al., 2015). Intracerebral neocortical recordings of calcarine cortex (Marzano et al., 2013) suggest that theta oscillations were the main oscillatory activity in this part of the cortex. We speculate the theta activity in calcarine, precuneus and adjacent areas of the occipital cortex might reflect mental imagery associated with sleep onset, called hypnagogic hallucinations. The fact that these oscillations are rather slow might indicate that they have an endogenous instead of an exogenous origin (it might have to do with visual fantasies rather than visual processing of an actual visual experience). However, in recovery additional frontal areas revealed increased theta activity. Thus, theta activity at the transition into sleep, particularly under increased sleep pressure might reflect a similar process as theta activity during prolonged wakefulness (Finelli et al., 2000; Hung et al., 2013).

Beta activity (16–24 Hz) gradually diminished in the course of SO and might reflect a gradual reduction of arousal (Marzano et al., 2013). This behavior has also been observed in other studies (De Gennaro et al., 2001a, 2005). The exponential decay was quicker in recovery; hence, the higher homeostatic pressure was also reflected at fast frequencies. Areas displaying the most prominent beta activity comprised parieto-occipital regions with some frontal contributions.

4.4. Definition of SO

As mentioned in the introduction, different definitions have been adopted to operationalize the SO process. This poses a problem when comparing the different studies, in particular if the temporal evolution of the SO process is considered. There is probably a general consensus that falling asleep is a gradual process that unfolds continuously as a function of time. However, for the analyses of the temporal evolution in a population, data must be aligned. Thus, there is an urgent need to find a broadly accepted definition of beginning and end of the SO period to make future investigations of the transition into sleep fruitful. Furthermore, future studies should investigate whether falling asleep at the beginning of sleep or after awakening during a sleep episode is the same or a similar process.

4.5. Limitations

Some limitations of the current analysis are important to note. For one, we could not address subcortical contributions, as the solution space is limited to the cortex (Pascual-Marqui et al., 1994, Pascual-Marqui 2002). Furthermore, subcortical components are often too weak to contribute directly to the EEG measured at the scalp level (Pascual-Marqui, 2002; Pascual-Marqui et al., 2011). We considered applying a new approach (Krishnaswamy et al., 2017) which claims that subcortical sources can be distinguished from cortical ones when the underlying cortical activity is sparse (i.e., limited to a subset of cortical regions). Yet, we decided against this approach, given the wide spread cortical activity of slow waves in sleep. However, at a subcortical level, hippocampal sleep spindles were detected minutes before sleep was scored at the scalp level (Sarasso et al., 2014) and the thalamus was deactivated before cortical areas (Magnin et al., 2010).

Further, 27 EEG electrodes were used which is at the lower limit for source localization and a general head model was employed. An additional limitation is the relatively small, homogenous sample of eight healthy good sleepers included in the analyses. Significant topographic differences due to sleep deprivation were reported in the original papers (Finelli et al., 2000, 2001a, 2001b), but it cannot be excluded that statistical power was insufficient. Nevertheless, we observed changes congruent to published findings.

5. Conclusions

LORETA proved to be a valuable tool to reveal the cortical sources underlying brain oscillatory activity at the transition into sleep. Classical EEG frequency bands exhibited location dependent brain dynamics during the SO transition, indicating that different brain areas are falling asleep at a different speed (Magnin et al., 2010; Marzano et al., 2013), reflecting varying levels of sleep pressure that built up during the day probably related to use dependent aspects of sleep regulation.

BA 11 was the most relevant brain region associated with delta activity, both in baseline and recovery (the latter condition reaching much stronger intensity levels). The dynamics of spindle activity resembled in both conditions an inverted U-shape with the maximum of activity shifted closer to SO in recovery sleep and an impaired capacity to sustain spindle activity.

Acknowledgements

We thank Drs. Leila Tarokh and Pascal Faber for comments on the manuscript.

Funding: This project was supported by the Swiss National Science Foundation, Switzerland, grant 32003B_146643.

Declarations of interest

None.

Appendix A. Supplementary material

Supplementary data associated with this article can be found in the online version at doi:10.1016/j.nbscr.2018.11.001.

References

Aeschbach, D., Borbély, A.A., 1993. All-night dynamics of the human sleep EEG. J. Sleep Res. 2, 70–81.
Aeschbach, D., Dijk, D.J., Borbély, A.A., 1997. Dynamics of EEG spindle frequency activity during extended sleep in humans: relationship to slow-wave activity and time of day. Brain Res. 748, 131–136.
Anderer, P., Klosch, G., Gruber, G., et al., 2001. Low-resolution brain electromagnetic tomography revealed simultaneously active frontal and parietal sleep spindle sources in the human cortex. Neuroscience 103, 581–592.
Berry, D.T.R., 1996. Sleep onset: normal and abnormal processes - Ogilvie, RD, Harsh, JR. Contemp. Psychol. 41, 495–496.
Borbély, A.A., Baumann, F., Brandeis, D., Strauch, I., Lehmann, D., 1981. Sleep-deprivation - effect on sleep stages and EEG power density in man. Electroencephalogr. Clin. Neurophysiol. 51, 483–493.
Brazier, M. a B., 1949. The electrical fields at the surface of the head during sleep. Electroencephalogr. Clin. Neurophysiol. 1, 195–204.
De Gennaro, L., Ferrara, M., 2003. Sleep spindles: an overview. Sleep. Med. Rev. 7, 423–440.
De Gennaro, L., Ferrara, M., Ferlazzo, F., Bertini, M., 2000. Slow eye movements and EEG power spectra during wake-sleep transition. Clin. Neurophysiol. 111, 2107–2115.
De Gennaro, L., Ferrara, M., Bertini, M., 2001a. The boundary between wakefulness and steep: quantitative electroencephalographic changes during the sleep onset period. Neuroscience 107, 1–11.
De Gennaro, L., Ferrara, M., Curcio, G., Cristiani, R., 2001b. Antero-posterior EEG changes during the wakefulness-sleep transition. Clin. Neurophysiol. 112, 1901–1911.
De Gennaro, L., Vecchio, F., Ferrara, M., Curcio, G., Rossini, P.M., Babiloni, C., 2004. Changes in fronto-posterior functional coupling at sleep onset in humans. J. Sleep. Res. 13, 209–217.
De Gennaro, L., Vecchio, F., Ferrara, M., Curcio, G., Rossini, P.M., Babiloni, C., 2005. Antero-posterior functional coupling at sleep onset: changes as a function of increased sleep pressure. Brain Res. Bull. 65, 133–140.
Del Felice, A., Arcaro, C., Storti, S.F., Fiaschi, A., Manganotti, P., 2014. Electrical source imaging of sleep spindles. Clin. EEG Neurosci. 45, 184–192.
Dijk, D.J., Brunner, D.P., Borbely, A.A., 1990. Time course of EEG power-density during long sleep in humans. Am. J. Physiol. 258, R650–R661.
Ferrara, M., De Gennaro, L., 2011. Going local: insights from EEG and stereo-EEG studies of the human sleep-wake cycle. Curr. Top. Med. Chem. 11, 2423–2437.
Finelli, L.A., Baumann, H., Borbély, A.A., Achermann, P., 2000. Dual electroencephalogram markers of human sleep homeostasis: correlation between theta activity in waking and slow-wave activity in sleep. Neuroscience 101, 523–529.
Finelli, L.A., Achermann, P., Borbély, A.A., 2001a. Individual “fingerprints” in human sleep EEG topography. Neuropsychopharmacology 25, S57–S62.
Finelli, L.A., Borbély, A.A., Achermann, P., 2001b. Functional topography of the human nonREM sleep electroencephalogram. Eur. J. Neurosci. 13, 2282–2290.
Hori, T., 1985. Spatiotemporal changes of EEG activity during waking-sleeping transition period. Int. J. Neurosci. 27, 101–114.
Hung, C.S., Sarasso, S., Ferrarelli, F., et al., 2013. Local experience-dependent changes in the wake EEG after prolonged wakefulness. Sleep 36, 59–72.
Iber, C., Ancoli-Israel, S., Chesson, A.L., Quan, S.F., 2007. The AASM Manual for the Scoring of Sleep and Associated Events: Rules, Terminology and Technical Specifications. American Academy of Sleep Medicine, Westchester, Illinois, USA.
Ikeda, S., Mizuno-Matsumoto, Y., Canuet, L., et al., 2015. Emotion regulation of neuroticism: emotional information processing related to psychosomatic state evaluated by electroencephalography and exact low-resolution brain electromagnetic tomography. Neuropsychobiology 71, 34–41.
Krishnaswamy, P., Obregon-Henao, G., Ahveninen, J., et al., 2017. Sparsity enables estimation of both subcortical and cortical activity from MEG and EEG. Proc. Natl. Acad. Sci. USA 114, E10465–E10474.
Magnin, M., Rey, M., Bastuji, H., Guillemant, P., Mauguiere, F., Garcia-Larrea, L., 2010. Thalamic deactivation at sleep onset precedes that of the cerebral cortex in humans. Proc. Natl. Acad. Sci. USA 107, 3829–3833.
Magosso, E., Ursino, M., Provini, F. and Montagna, P. Wavelet analysis of electroencephalographic and electro-oculographic changes during the sleep onset period. In: Proceedings of Annual International Conference of the IEEE Engineering in Medicine and Biology Society, Vols 1–16, 2007:4006-10.
Marzano, C., Moroni, F., Gorgoni, M., Nobili, L., Ferrara, M., De Gennaro, L., 2013. How we fall asleep: regional and temporal differences in electroencephalographic synchronization at sleep onset. Sleep Med. 14, 1112–1122.
Merica, H., Gaillard, J.M., 1992. The EEG of the sleep onset period in insomnia – a discriminant analysis. Physiol. Behav. 52, 199–204.
Nichols, T.E., Holmes, A.P., 2002. Nonparametric permutation tests for functional neuroimaging: a primer with examples. Hum. Brain Mapp. 15, 1–25.
Nir, Y., Staba, R.J., Andrillon, T., et al., 2011. Regional slow waves and spindles in human sleep. Neuron 70, 153–169.
Ogilvie, R.D., 2001. The process of falling asleep. Sleep. Med. Rev. 5, 247–270.
Olbrich, E., Achermann, P., 2005. Analysis of oscillatory patterns in the human sleep EEG using a novel detection algorithm. J. Sleep. Res. 14, 337–346.
Park, D.H., Ha, J.H., Ryu, S.H., Yu, J., Shin, C.J., 2015. Three-dimensional electroencephalographic changes on Low-Resolution Brain Electromagnetic Tomography (LORETA) during the sleep onset period. Clin. EEG Neurosci. 46, 340–346.
Parrino, L., Ferri, R., Zucconi, M., Fanfulla, F., 2009. Commentary from the Italian Association of Sleep Medicine on the AASM manual for the scoring of sleep and associated events: for debate and discussion. Sleep Med. 10, 799–808.
Pascual-Marqui, R., 2002. Standardized low-resolution brain electromagnetic tomography (sLORETA): technical details. Methods Find. Exp. Clin. Pharmacol. 24, 5–12.
Pascual-Marqui, R., Biscay, R., Bosch-Bayard, J., et al., 2014a. Assessing direct paths of intracortical causal information flow of oscillatory activity with the isolated effective coherence (iCoh). Front. Hum. Neurosci. 8.
Pascual-Marqui, R.D., Michel, C.M., Lehmann, D., 1994. Low-resolution electromagnetic tomography – a new method for localizing electrical activity in the brain. Int. J. Psychophysiol. 18, 49–65.
Pascual-Marqui, R.D., Esslen, M., Kochi, K., Lehmann, D., 2002. Functional imaging with low-resolution brain electromagnetic tomography (LORETA): a review. Methods Find. Exp. Clin. Pharmacol. 24, 91–95.
Pascual-Marqui, R.D., Lehmann, D., Koukkou, M., et al., 2011. Assessing interactions in the brain with exact low-resolution electromagnetic tomography. Philos. Trans. R. Soc. A-Math. Phys. Eng. Sci. 369, 3768–3784.
Pascual-Marqui, R.D., Rolando, J.B., Bosch-Bayard, J., et al., 2014b. Advances in EEG methods applied to intra-cortical connectivity inference and to functional imaging: examples in psychiatry research. Int. J. Psychophysiol. 94 (121-121).
Picchioni, D., Fukunaga, M., Carr, W.S., et al., 2008. fMRI differences between early and late stage-1 sleep. Neurosci. Lett. 441, 81–85.
Prerau, M.J., Hartnack, K.E., Obregon-Henao, G., et al., 2014. Tracking the sleep onset process: an empirical model of behavioral and physiological dynamics. Plos Comput. Biol. 10.
Rechtschaffen, A., Kales, A., 1968. A Manual of Standardized Terminology, Techniques and Scoring System of Sleep Stages in Human Subjects. Brain Information Service/Brain Research Institute, University of California, Los Angeles.
Rogers, R.D., Owen, A.M., Middleton, H.C., et al., 1999. Choosing between small, likely rewards and large, unlikely rewards activates inferior and orbital prefrontal cortex. J. Neurosci. 19, 9029–9038.
Rusterholz, T., Achermann, P., 2011. Topographical aspects in the dynamics of sleep homeostasis in young men: individual patterns. BMC Neurosci. 12, 84.
Sarasso, S., Proserpio, P., Pigorini, A., et al., 2014. Hippocampal sleep spindles preceding neocortical sleep onset in humans. Neuroimage 86, 425–432.
Scheuler, W., Kubicki, S., Marquardt, J., Scholz, G., Weiss, K., Henkes, H., Gaeth, L., 1988. The α-sleep pattern – quantitative analysis and functional aspects. In: Koella, W.P., Obal, F., Schulz, H., Visser, P. (Eds.), Sleep ‘86. Gustav Fischer Verlag, New York, pp. 284–286.
Scheuler, W., Rappelsberger, P., Pastelakprice, C., Kubicki, S., Petsche, H., 1993. Alpha-activity of NREM sleep. Basic Mech. EEG 183–214.
Siclari, F., Bernardi, G., Riedner, B.A., Larocque, J.J., Benca, R.M., Tononi, G., 2014. Two distinct synchronization processes in the transition to sleep: a high-density electroencephalographic study. Sleep 37, 1621–1637.
Speth, C., Speth, J., 2016. The borderlands of waking: quantifying the transition from reflective thought to hallucination in sleep onset. Conscious. Cogn. 41, 57–63.

Spiess, M., Bernardi, G., Kurth, S., et al., 2018. How do children fall asleep? A high-density EEG study of slow waves in the transition from wake to sleep. Neuroimage 178, 23–35.
Vecchio, F., Miraglia, F., Gorgoni, M., et al., 2017. Cortical connectivity modulation during sleep onset: a study via graph theory on EEG data. Human. Brain Mapp. 38, 5456–5464.
Vogt, B.A., Laureys, S., 2005. Posterior cingulate, precuneal and retrosplenial cortices: cytology and components of the neural network correlates of consciousness. Boundaries Conscious.: Neurobiol. Neuropathol. 150, 205–217.
Wright, K.P., Badia, P., Wauquier, A., 1995. Topographical and temporal patterns of brain activity during the transition from wakefulness to sleep. Sleep 18, 880–889.